

# The Velocity Distribution of the Nearest Interstellar Gas

Priscilla C. Frisch

Lauren Grodnicki

Daniel E. Welty

*University of Chicago, Department of Astronomy and Astrophysics, 5460 S. Ellis Avenue,  
Chicago, IL 60637*

## ABSTRACT

The bulk flow velocity for the cluster of interstellar cloudlets within  $\sim 30$  pc of the Sun is determined from optical and ultraviolet absorption line data, after omitting from the sample stars with circumstellar disks or variable emission lines and the active variable HR 1099. Ninety-six velocity components towards the remaining 60 stars yield a streaming velocity through the local standard of rest of  $-17.0 \pm 4.6$  km s $^{-1}$ , with an upstream direction of  $l^{\text{II}}=2.3^\circ$ ,  $b^{\text{II}}=-5.2^\circ$  (using *Hipparcos* values for the solar apex motion). The velocity dispersion of the interstellar matter (ISM) within 30 pc is consistent with that of nearby diffuse clouds, but present statistics are inadequate to distinguish between a Gaussian or exponential distribution about the bulk flow velocity. The upstream direction of the bulk flow vector suggests an origin associated with the Loop I supernova remnant. Groupings of component velocities by region are seen, indicating regional departures from the bulk flow velocity or possibly separate clouds. The absorption components from the cloudlet feeding ISM into the solar system form one of the regional features. The nominal gradient between the velocities of upstream and downstream gas may be an artifact of the Sun's location near the edge of the local cloud complex. The Sun may emerge from the surrounding gas-patch within several thousand years.

## 1. Introduction

A number of studies have searched for correlations between the velocity of interstellar gas observed inside the solar system and towards external stars (Adams & Frisch 1977;

McClintock et al. 1978; Lallement & Bertin 1992). Adams & Frisch (1977) showed that the velocity of interstellar gas inside the solar system differs by several  $\text{km s}^{-1}$  from interstellar cloud velocities towards stars located in the upstream direction. The discovery that the  $\text{H}^{\circ}$   $\text{L}\alpha$  line is redshifted by several  $\text{km s}^{-1}$  from the  $\text{D}^{\circ}$  line towards the nearest star ( $\alpha$  Cen, 1.3 pc) confused the identification of the cloud velocity in this direction (Landsman et al. 1984). This shift has since been successfully modeled by including the  $\text{L}\alpha$  absorption from compressed  $\text{H}^{\circ}$  in the heliosheath (Linsky & Wood 1996; Gayley et al. 1997). However, the heliosheath is observed only in the strong  $\text{L}\alpha$  line. The  $\text{D}^{\circ}$ ,  $\text{Mg}^+$ , and  $\text{Fe}^+$  line velocities towards  $\alpha$  Cen ( $\sim -19 \text{ km s}^{-1}$ , Lallement et al. 1995; Linsky & Wood 1996) disagree by  $\sim 2 \text{ km s}^{-1}$  with interstellar gas and dust velocities found inside the solar system (e.g. Weller & Meier 1981; Witte et al. 1996; Flynn et al. 1998; Frisch et al. 1999) when projected towards  $\alpha$  Cen. Optical and ultraviolet (UV) data show that the bulk flow of the closest interstellar material (ISM) has an upstream direction towards the Loop I supernova remnant, and a velocity  $\sim 20 \text{ km s}^{-1}$  in the local standard of rest (LSR) (Frisch 1981; Crutcher 1982; Frisch 1995). This bulk flow is similar to ISM expanding around OB associations (e.g. Münch 1957). Following Slavin & Frisch (2002, hereafter SF02), the ISM within 30 pc is referred to as the complex of local interstellar clouds (CLIC), while the cloudlet feeding ISM into the solar system is denoted the Local Interstellar Cloud (LIC). Optical  $\text{Ca}^+$  and UV absorption data show that the CLIC is inhomogeneous on subparsec scales, and that multiple absorption components are present towards the nearest stars (e.g. Munch & Unsold 1962; Ferlet et al. 1986; Lallement et al. 1986; Vallerga et al. 1993; Lallement et al. 1994; Crawford & Dunkin 1995; Welty et al. 1996; Frisch 1995, 1996; Crawford et al. 1997, 1998). The kinematics of the CLIC provides the opportunity to probe the history of a diffuse cloud, the relevance of small scale structure to ISM physics, and to gauge the past and future galactic environment of the Sun (Frisch 1997).

Nearby ISM provides a unique set of constraints for determining diffuse cloud physics. Observations of both pickup ions inside the solar system (formed by interactions of interstellar neutrals with the solar wind) and interstellar absorption lines towards nearby stars have been used to constrain the first full radiative transfer model of nearby ISM (SF02). These results indicate that the interstellar properties at the solar location are  $T \sim 7,000 \text{ K}$ ,  $n(\text{H}^{\circ}) \sim 0.24 \text{ cm}^{-3}$ ,  $n(\text{e}^{-}) \sim 0.13 \text{ cm}^{-3}$ , and fractional ionizations  $X(\text{H}) \sim 31\%$  and  $X(\text{He}) \sim 48\%$ , with both density and ionization levels varying towards the cloud surface (Model 17). The model includes emission from a conductive interface, which yields an excess of helium compared to hydrogen ionization (SF02). If the density  $n(\text{H}^{\circ}) \sim 0.24 \text{ cm}^{-3}$  is typical for all cloudlets near the Sun, then  $N(\text{H}^{\circ})$  towards  $\alpha$  Cen (1.3 pc, Linsky & Wood 1996) suggests a filling factor  $f \sim 0.4$ . Enhanced refractory element abundances in warm nearby gas provide evidence that local ISM has been shocked (Frisch et al. 1999). The presence of cold  $\text{Ca}^+$  and  $\text{Na}^{\circ}$  absorp-

tion components (Doppler width  $b_D \leq 0.8 \text{ km s}^{-1}$ ) towards  $\alpha$  Pav (56 pc) and  $\delta$  Cyg (52 pc) indicate at least an order of magnitude variation for ISM temperatures within 50 pc (see references in Table 3).

The sensitivity of heliosphere properties (Zank & Frisch 1999) — and astrospheres in general (including extra-solar planetary systems, Frisch 1993) — to the physical conditions of the surrounding ISM motivates this exploration of small scale structure in the nearby ISM using cloud velocity as a structure proxy. Understanding small scale structure in the CLIC will also help decipher the signature that astrospheres leave on the interstellar H $\alpha$  Ly $\alpha$  absorption line. This paper focuses on the bulk flow kinematics of ISM within  $\sim 30$  pc of the Sun. Anticipating a conclusion, the CLIC appears to consist of an ensemble of cloudlets at velocities consistent with a random distribution about a mean bulk flow velocity. The first results of this study were presented by Frisch (2001).

## 2. Velocities of Absorption Components

### 2.1. Method

In this analysis we assume that the motions of nearby interstellar clouds (i.e. the CLIC) in the local standard of rest (LSR) can be described by a linear flow vector,  $\vec{V}_{\text{flow}}$ , which is characterized by the flow velocity and the galactic coordinates of the direction from which the gas flows (implying that the flow velocity is  $< 0$ ). Our approach is to calculate a best fitting flow vector for a set of observed interstellar cloud component radial velocities which sample interstellar gas within  $\sim 30$  pc (Section 2.2), and then to determine the distribution of component velocities about this bulk flow vector. If the CLIC ( $d < 30$  pc) is part of an expanding shell feature from Loop I (Section 3.1), it will subtend a total angle equivalent to about 10% of the expanding shell and yield  $< 5\%$  deviations from a linear flow velocity (i.e.  $\sim 1 \text{ km s}^{-1}$  for uniform expansion). Therefore, over the scale length of the CLIC, the linear assumption is sufficient. The bulk flow velocity vector is determined from a fitting procedure that varies  $\vec{V}_{\text{flow}}$  in order to minimize the sum,  $\Phi_m$ , over  $m$  observed interstellar absorption line components, of the square of the difference between the projected flow and observed velocity towards each star, i.e., to minimize:

$$\Phi_m = \sum_{i=1}^m dV_i^2, \quad (1)$$

where

$$dV_i = v_{i,\text{obs}} - \vec{V}_{\text{flow}} \cdot \hat{k}_{\text{star}}. \quad (2)$$

For a flow vector calculated from a set of  $m$  components ( $\vec{V}_{\text{flow}}(m)$ ),

$$dV_i(m) = v_{i,\text{obs}} - \vec{V}_{\text{flow}}(m) \cdot \hat{k}_{\text{star}}, \quad (3)$$

where  $dV_i(m)$  is the scalar radial velocity (at the solar location) of component  $i$  in the rest frame of  $\vec{V}_{\text{flow}}(m)$ . Here  $\hat{k}_{\text{star}}$  is the unit position vector towards each star and  $v_{i,\text{obs}}$  is the observed heliocentric (HC) radial velocity for an interstellar velocity component towards that star (here denoted  $i$ , where  $i=1,m$ ). The fits were performed using the FindMin function in Mathematica, which determined the local minima of the function  $\Phi_m$  as a function of the three variables  $V,l,b$  which define  $\vec{V}_{\text{flow}}$ . Note that since many stars show more than one interstellar absorption component, the number of components ( $m$ ) is greater than the number of stars. An unweighted fit was employed since there is no obvious weighting function. Line broadening is not suitable since instrument resolutions and thermal broadening vary (artificially blending velocity components). Column densities are unsuitable since they vary between species. Note that since we are interested in the distribution of the deviation of component velocities in the rest frame of  $\vec{V}_{\text{flow}}$ , the component data set includes all measured components for each star. We find that this procedure yields a predicted flow velocity,  $\vec{V}_{\text{flow}}$ , which is relatively insensitive to the detailed set of the selected velocity components, provided that sky coverage is good and that several stars with components at anomalous velocities are removed from the sample (next section).

In principle, the full three-dimensional flow vector  $\vec{V}_{\text{flow}}$  is calculated correctly for cases where the perturbations from the flow ( $dV_i$ ) are random, since the Sun is immersed in the flow. Alternative cases whereby perturbations in the flow have a directional dependence (or preference), or where the flow is decelerated (Frisch 1995), are not considered here. However, we make an elementary attempt to identify systematic regional patterns in the velocity components.

## 2.2. Component Set and Bulk Velocity

The velocities of optical and ultraviolet absorption lines towards nearby stars, and towards more distant stars which sample primarily the CLIC gas, are used to evaluate the velocity distribution of the CLIC. Interstellar absorption line data for 67 stars which sample the CLIC are listed in Table 2, with component information in Table 3. This component set forms the “unrestricted sample”. A range of data sources was used in order to cover as much of the sky as possible. Observations of the optical interstellar  $\text{Ca}^+$  lines represent the primary source of cloud velocity data, but the optical data do not adequately sample the downstream region where column densities are low over the first  $\sim 30$  pc (e.g.  $N(\text{Ca}^+) \ll 10^{10} \text{ cm}^{-2}$ ,

Bruhweiler & Kondo 1982; Frisch & York 1983; Frisch 1995; Lallement et al. 1995). Observations of the intrinsically stronger UV lines of  $\text{Fe}^+$ ,  $\text{Mg}^+$ ,  $\text{D}^\circ$ , and  $\text{H}^\circ$  are available for several stars in the downwind direction and towards the north galactic pole (where column densities are also low).

The component sample results primarily from fits to optical and UV absorption lines observed at relatively high resolution ( $<3 \text{ km s}^{-1}$ ); medium resolution UV data were used for a few stars. When both optical and UV data exist, the optical  $\text{Ca}^+$  data (resolution  $0.5\text{--}3 \text{ km s}^{-1}$ ) are the first choice, and the UV data second choice since about 50% of the optical spectra were acquired with resolution  $\text{FWHM} < 1.5 \text{ km s}^{-1}$ . Component velocities are generally obtained from a process which iteratively fits each discernible component in the absorption line profile with a population of atoms with a Maxwellian velocity distribution about the central component velocity, with a projection in the radial line-of-sight towards the Sun of  $v_{\text{obs}}$  (denoted  $v_{i,\text{obs}}$  in eqs. 2, 3). The number of components and the component descriptors (column density,  $v_{\text{obs}}$ , and Doppler broadening constant,  $b_{\text{D}}$ ) are sensitive to instrument resolution and signal-to-noise and to the judgment of the observer.

The component sample used here is not of uniform quality. For example, the star  $\alpha$  Oph (14 pc) has been observed at resolutions of  $0.3 \text{ km s}^{-1}$  by Crawford & Dunkin (1995) and  $1.2 \text{ km s}^{-1}$  Welty et al. (1996). The  $0.3 \text{ km s}^{-1}$  resolution profiles were fitted with four components with velocities  $-32.0 \pm 0.5$ ,  $-28.4 \pm 0.3$ ,  $-26.2 \pm 0.2$  and  $-23.6 \pm 0.5 \text{ km s}^{-1}$ . The  $1.2 \text{ km s}^{-1}$  resolution profiles were fitted with three components with velocities  $-33.03 \text{ km s}^{-1}$ ,  $-26.25 \text{ km s}^{-1}$ ,  $-22.16 \text{ km s}^{-1}$ . While temporal variations in interstellar  $\text{Ca}^+$  absorption profiles are seen in a few cases (e.g. Hobbs et al. 1991), comparisons between the two absorption profiles suggest that the component at  $-28.4 \text{ km s}^{-1}$  was unresolved in the lower resolution data.

The derived flow vector depends on the component set used in the fitting procedure, and the unrestricted sample is small enough that lines incorrectly identified as interstellar may alter the results. Therefore, the basic star sample was restricted to omit stars with either identified circumstellar disks or strong emission line spectra (where misidentification of circumstellar features is possible). Thus the stars  $\epsilon$  Eri (3.2 pc),  $\beta$  Pic (19.3 pc),  $\beta$  Leo (11.0 pc),  $\alpha$  Lyr (7.6 pc),  $\alpha$  PsA (7.7 pc), which have circumstellar disks identified at  $60 \mu\text{m}$  (e.g. Habing et al. 2001), were omitted from the sample. Although interstellar components can in principle be distinguished from circumstellar disk components since stellar velocities are known, we considered the sample to be more reliable when stars with circumstellar disks are omitted. The emission line star  $\alpha$  Eri (44 pc) was also omitted, as it shows variable  $\text{He}^\circ$  and  $\text{Mg}^+$  chromospheric features indicating that weak circumstellar absorption features may be present. The active RS CVn variable HR 1099 (Wood et al. 1996b) was also omitted from

the sample because the inclusion of the components towards this star yielded results that are inconsistent with fits towards the other stars (see below). With the above omissions, the remaining restricted sample consists of 60 stars with a total of 96 components. Star distances range from 1.3 pc ( $\alpha$  Cen) to 132 pc ( $\epsilon$  CMa). Components towards the two stars beyond 70 pc,  $\epsilon$  CMa and 31 Com, were included because these stars primarily sample ISM within 30 pc (Gry & Jenkins 2001; Dring et al. 1997) and fill a gap in the spatial coverage.

This basic component sample was fitted for the flow vector  $\vec{V}_{\text{flow}}$ , yielding a HC vector  $\vec{V}_{\text{flow}}(96)$  with radial velocity  $-28.1 \pm 4.6$  km s $^{-1}$ , flowing from the upstream direction  $l^{\text{II}}=12.4^\circ$ ,  $b^{\text{II}}=11.6^\circ$ . The uncertainty is the 1- $\sigma$  value of the velocity component distribution about the bulk flow velocity. Figure 1a shows the deviations  $dV_i(96)$  plotted against the stellar distance (omitting the two stars more distant than 70 pc). Note that 76 of these 96 components originate in the upstream direction, while the remaining components originate downstream, reflecting the higher column densities of nearby ISM found upstream (e.g., Frisch 1995).

The positions of the stars forming the 96 component set are plotted in Figure 2a. Most of the sky is well sampled, except for the interval  $l^{\text{II}}=150^\circ$ – $180^\circ$  in the direction of the third galactic quadrant void (also known as the Puppis window or the  $\beta$  CMa tunnel), where mean interstellar column densities are low out to  $\sim 100$  pc ( $\overline{n_{\text{H}^0}} < 0.003$  cm $^{-3}$ ). Figure 3a shows  $dV_i(96)$  as a function of the galactic longitude of the star; no strong systematic spatial dependence is seen. For comparison, the LSR velocities of the 96 components ( $dV_i(\text{LSR})$ ) are plotted against galactic longitude in Figure 3b, illustrating the expected behavior for an incorrect vector describing the flow. Throughout this paper we use the solar apex motion based on *Hipparcos* data, corresponding to a solar motion towards the galactic coordinates  $l^{\text{II}}=27.7^\circ$ ,  $b^{\text{II}}=32.4^\circ$  at the velocity  $V=13.4$  km s $^{-1}$  (Dehnen & Binney 1998).

The robustness of  $\vec{V}_{\text{flow}}(96)$  was tested in several ways. The first test was to restrict the star sample to stars within 29 pc of the Sun (except for  $\epsilon$  CMa and 31 Com, which sample the nearest ISM and are required for completeness in low column density directions). This restriction gives 46 components towards 31 stars. The best fit HC flow vector for this 46 component sample,  $\vec{V}_{\text{flow}}(46)$ , corresponds to an upstream direction of  $l^{\text{II}}=12.5^\circ$ ,  $b^{\text{II}}=12.5^\circ$ , with an inflow velocity of  $-28.1 \pm 4.3$  km s $^{-1}$ . The fact that  $\vec{V}_{\text{flow}}(46)$  is virtually identical to  $\vec{V}_{\text{flow}}(96)$  is not a coincidence, since the initial selection of stars in Table 3 was restricted to stars which did not appear to contain neutral ISM more distant than  $\sim 30$  pc. The closeness of the  $\vec{V}_{\text{flow}}(96)$  and  $\vec{V}_{\text{flow}}(46)$  vectors support the validity of eliminating HR 1099 from the component sample, since had HR 1099 been retained in the restricted sample the resulting fitted vector ( $\vec{V}_{\text{flow}}(99)$ ) would have differed from  $\vec{V}_{\text{flow}}(46)$  by 0.6 km s $^{-1}$  and  $2^\circ$ .

The second test was a search for spatially correlated variations in  $dV_i(96)$ . Star posi-

tions are replotted in Figure 2b, with symbols coded for  $dV_i(96)$ . No systematic positional dependence appears for components with  $|dV_i(96)| > 5 \text{ km s}^{-1}$ . However, when the components with  $|dV_i(96)| < 5 \text{ km s}^{-1}$  are plotted with symbols which code the sign of  $dV_i(96)$ , stars in the interval  $l^{\text{II}}=150^\circ \rightarrow 250^\circ$  are found to show components with systematically small but negative  $dV_i(96)$  values (Figure 2c, note several components are overplotted). The best-fitting flow vector,  $\vec{V}_{\text{flow}}(20)$ , for the 20 components toward 14 stars located in the interval  $l^{\text{II}}=150^\circ \rightarrow 250^\circ$  corresponds to a vector velocity  $-25.8 \pm 4.3 \text{ km s}^{-1}$  from the upstream direction  $l^{\text{II}}=6.2^\circ$ ,  $b^{\text{II}}=10.4^\circ$ . If only a single component per star is selected for the fit, biasing towards components with small  $dV_i(\text{He})$  values, the resulting fitted vector  $\vec{V}_{\text{flow}}(20)$  corresponds to a velocity  $-25.6 \pm 1.3 \text{ km s}^{-1}$  from the upstream direction  $l^{\text{II}}=6.4^\circ$ ,  $b^{\text{II}}=13.1^\circ$ , which is close to  $\vec{V}_{\text{flow}}(\text{He})$  (Table 1, Section 3.3.1). Gas near the LIC velocity (Table 1) dominates in the downwind direction ( $l \sim 180^\circ$ ), as found previously. The LIC and other regional variations in  $\vec{V}_{\text{flow}}(96)$  are discussed in Section 3.3.

### 2.3. Component Velocity Dispersion

The randomness of interstellar cloud velocities has long been of considerable interest, with early arguments presented for random motions of  $\sim 20 \text{ km s}^{-1}$  for interstellar particles (Spitzer 1942), compared to recent data showing root-mean-square velocity dispersions of  $\sim 0.5 \text{ km s}^{-1}$  in individual cold clouds. Early studies of diffuse cloud kinematics found an exponential distribution for cloud velocities, suggestive of a turbulent ISM (Blaauw 1952; Münch 1957).

The functional form of the velocity distribution of the CLIC gas was tested, but the results prove inconclusive. A plot of the number of components (N, ordinate) binned for a given value of  $dV_i(96)$  (abscissa) is shown in Figure 4. Here, N is determined with  $dV_i(96)$  binned with  $1 \text{ km s}^{-1}$  bin sizes. The histogram is “noisy” because the sample is small.

For a purely random distribution of individual components about the central flow velocity  $\vec{V}_{\text{flow}}(96)$ , the form of the  $dV_i$  distribution should be Gaussian:

$$\Psi(V) = \frac{c_g}{b\sqrt{\pi}} \exp - (V - V_o)^2/b^2 \quad (4)$$

The Blaauw (1952) and Münch (1957) results for  $\text{Ca}^+$  and  $\text{Na}^o$  lines, based on low resolution data ( $\text{FWHM} > 5 \text{ km s}^{-1}$ ), are consistent with an exponential distribution for cloud velocities:

$$\Psi(V) = \frac{c_e}{2\eta} \exp - |V - V_o|/\eta, \quad (5)$$

such as is expected for a turbulent flow. Here,  $b = \sigma\sqrt{2}$ ,  $c_g$  and  $c_e$  are normalizing constants, and  $\sigma$  and  $\eta\sqrt{2}$  are the root-mean-square deviations of the Gaussian and exponential

distributions respectively.

The 96 component sample was tested for the distribution of  $dV_i(96)$ , assuming alternatively Gaussian and exponential distributions. The best-fit Gaussian distribution yields  $b^{\text{II}}=6.2 \text{ km s}^{-1}$ , and the best-fit exponential distribution yields  $\eta=5.1 \text{ km s}^{-1}$ . The present data do not distinguish between these two distributions (see overplotted functions in Figure 4). Blaauw concluded that an exponential function with mean speed  $\eta \sim 5 \pm 1 \text{ km s}^{-1}$  provided the best fit to  $\text{Ca}^+$  K-line data towards 300 stars observed by Adams (1949) with instrumental resolution  $\sim 9 \text{ km s}^{-1}$ . Munch inferred that an exponential form fit observations of the  $\text{Ca}^+$  and  $\text{Na}^\circ$  doublets towards 112 stars, with  $\eta \sim 5\text{--}6 \text{ km s}^{-1}$  for  $\text{Ca}^+$  in the Orion arm and a somewhat smaller value for  $\text{Na}^\circ$ . Munch concluded that turbulence dominates the velocity distribution of these components. These early low resolution data undersample blended components at low velocity and therefore probably enhance component statistics in the distribution wings with respect to the central region. It is therefore puzzling that we find a similar value from higher resolution data. This issue is discussed further in a subsequent paper (Frisch & Welty 2002).

### 3. Discussion

#### 3.1. Upstream Direction and Loop I

The best-fit heliocentric velocity vector,  $\vec{V}_{\text{flow}}(96)$ , corresponds to a bulk velocity  $-28.1 \text{ km s}^{-1}$  flowing from the upstream direction  $l^{\text{II}}=12.4^\circ$ ,  $b^{\text{II}}=11.6^\circ$  (Section 2.2). However in order to compare  $\vec{V}_{\text{flow}}(96)$  with morphological features in the astronomical sky the solar apex motion through the LSR must be subtracted. Subtracting the solar apex motion from  $\vec{V}_{\text{flow}}(96)$  gives a “true” upstream direction (in LSR) in galactic coordinates of  $l^{\text{II}}=2.3^\circ$ ,  $b^{\text{II}}=-5.2^\circ$ , with flow velocity  $-17.0 \text{ km s}^{-1}$ .<sup>1</sup> The  $\vec{V}_{\text{flow}}(96)$  upwind direction is shown plotted against the filamentary  $\text{H}^\circ$  structure associated with Loop I (21 cm data, Figure 5, Hartmann & Burton 1997). The position of the radio continuum Loop I shell, defined from the discovery 408 MHz radio continuum data, is marked (from Berkhuijsen 1971; Haslam et al. 1982).

Low column densities in the CLIC components ( $N(\text{H}) < 10^{18.5} \text{ cm}^{-2}$ , typically) prevent linking CLIC velocities to individual features in the 21-cm  $\text{H}^\circ$  sky maps. The relation between the flow of interstellar gas past the Sun and the Loop I superbubble has been discussed

---

<sup>1</sup>For comparison, the standard solar apex motion (based on the brightest stars with a range of ages) is  $19.7 \text{ km s}^{-1}$  towards  $l^{\text{II}}=57^\circ$ ,  $b^{\text{II}}=+22^\circ$ , which yields an upstream LSR flow motion of  $-19.4 \text{ km s}^{-1}$  from the direction  $l^{\text{II}}=331.4^\circ$ ,  $b^{\text{II}}=-4.9^\circ$ .

from several viewpoints (e.g. Frisch 1979, 1981; Crutcher 1982; Frisch 1995; Crawford 1991; de Geus 1992). The Loop I superbubble remnant (the brightest segment of which is the North Polar Spur) is centered near  $l^{\text{II}} \sim 320^\circ$ ,  $b^{\text{II}} \sim 5^\circ$ , with distance  $\sim 130$  pc and radius  $\sim 80^\circ$  (based on  $\text{H}^\circ$  21 cm data, Heiles 1998). The radio-continuum Loop I is centered at  $l^{\text{II}} = 329^\circ$ ,  $b^{\text{II}} = +17.5^\circ$ , radius  $58^\circ$ , and is strongly limb-brightened in the tangential direction near  $l^{\text{II}} \sim 35^\circ$  (Berkhuijsen 1973). The center of Loop I defined from  $\text{H}^\circ$  data is offset from the radio-continuum center by  $\sim 15^\circ$ . The  $\text{H}^\circ$  shell shows a polar cap at  $v_{\text{LSR}} \sim -30$  km s $^{-1}$  and  $l^{\text{II}}, b^{\text{II}} \approx 300^\circ, -10^\circ$  (Heiles 1989), where the cold component seen at  $-19.6$  km s $^{-1}$  towards  $\alpha$  Pav may originate (Table 3). This expansion velocity implies a projected velocity of  $\approx -14$  km s $^{-1}$  for the  $\vec{V}_{\text{flow}}(96)$  LSR upwind direction, versus the best-fit LSR velocity of  $-17.0$  km s $^{-1}$ . The filamentary structure and likely asymmetric expansion of the  $\text{H}^\circ$  shell make it difficult to identify the approaching portion of the  $\text{H}^\circ$  shell, so the  $\sim 20\%$  difference between the projected polar cap velocity and the LSR bulk velocity of the CLIC gas possibly is within uncertainties. However, the  $\text{H}^\circ$  shell regions traced by the 21-cm polar cap emission are denser and colder than the CLIC gas appears to be. Alternatively, models of shell expansion from the formation of the Sco-Cen Association Upper Scorpius subgroup place an  $\text{H}^\circ$  shell with LSR velocity  $\sim -22$  km s $^{-1}$  and age  $\sim 4$  Myrs at the solar location (Crawford 1991; de Geus 1992; Frisch 1995).<sup>2</sup>

### 3.2. Comparison with Previous Models

The bulk flow of nearby interstellar gas has been determined from optical absorption lines observed towards nearby stars (primarily  $\text{Ca}^+$ , e.g. Crutcher 1982; Frisch 1986; Lallement et al. 1986; Lallement & Bertin 1992; Vallerga et al. 1993; Frisch 1995, 1997). The velocity vectors determined from these earlier studies are summarized in Table 5. Since column densities in the downstream direction are low ( $\log[N(\text{H}^\circ)] < 18$  cm $^{-2}$ ), optical lines do not easily sample this interval. This causes bulk flow vectors based primarily on  $\text{Ca}^+$  data to be strongly weighted towards upstream gas and quite sensitive to the details of the star sample. The inclusion of UV data provides an adequate sample of downstream gas, but at lower resolution (3 km s $^{-1}$ ). Lallement & Bertin (1992, LB92) used UV data to identify the ISM in the downstream direction, denoting it the “anti-Galactic” cloud (AG, Table 5), which is the same as the LIC. ISM identified in the upstream direction, generally towards the galactic-center hemisphere, was denoted the “Galactic” cloud (G, Table 5). The velocity difference between the G and AG clouds is smaller than found by Adams & Frisch (1977,

---

<sup>2</sup>Note the age given for the most recent shell-forming event should be 4 Myrs, not 400,000 yrs (Frisch 1995, page 532).

based on backscattered  $L\alpha$   $H^{\circ}$  data) because of the deceleration and compression of  $H^{\circ}$  in the heliosheath regions (which was unknown in 1977). LB92 concluded that either the Sun is located in a patch of gas with velocity intermediate between the G and AG clouds, or that  $H^{\circ}$  is decelerated in the heliosheath (or both). The *Ulysses* He and 584 Å backscattering data confirm the velocity of ISM inside the solar system, so that the general velocity difference between the upstream and downstream ISM is real. However, the fact that the velocities of CLIC cloudlets are consistent with a random distribution about the mean bulk flow velocity suggests that the upstream/downstream velocity gradient locally displayed by the G versus LIC vectors may be an artifact of the location of the Sun with respect to the “edge” of the CLIC complex. Alternatively, the presence of a blue-shifted cloud towards CMa (Lallement et al. 1994; Gry & Jenkins 2001) is also consistent with a velocity gradient.

For comparison with the LB92 G-AG two-flow model, a separate bulk flow velocity was calculated for downstream components. The 20 LIC components originating in the interval  $l^{\text{II}}=150^{\circ}\rightarrow 250^{\circ}$  were removed from the 96 component sample. The fit to the resulting 76 components yields  $\vec{V}_{\text{flow}}(76)=-29.3\pm 4.0$  km s $^{-1}$ , from HC upstream direction  $l^{\text{II}}=13.1^{\circ}$ ,  $b^{\text{II}}=11.2^{\circ}$ . The velocities of  $\vec{V}_{\text{flow}}(76)$  and the G vector ( $\vec{V}_{\text{flow}}(\text{G})$ ) coincide, although the upstream directions differ by  $\sim 12^{\circ}$ . The observed 3.5 km s $^{-1}$  difference between  $\vec{V}_{\text{flow}}(76)$  and  $\vec{V}_{\text{flow}}(20)$  and the near coincidence of upwind directions (within  $\sim 8^{\circ}$ ) suggests a deceleration of the bulk flow. The two-flow model with the two vectors  $\vec{V}_{\text{flow}}(20)$  and  $\vec{V}_{\text{flow}}(76)$  (or alternatively with  $\vec{V}_{\text{flow}}(\text{He})$  and  $\vec{V}_{\text{flow}}(\text{G})$ ) is not a unique description of CLIC gas. For example, the velocity dispersion of  $\vec{V}_{\text{flow}}(76)$  is about equal to the difference between the  $\vec{V}_{\text{flow}}(76)$  and  $\vec{V}_{\text{flow}}(20)$  velocities ( $\sim 4$  km s $^{-1}$ ). The second shortcoming is that 6 stars in the  $l^{\text{II}}=150^{\circ}\rightarrow 250^{\circ}$  interval show two absorption components, and the second components are not accommodated by the two-flow model. The dispersion of the entire 20 components about  $\vec{V}_{\text{flow}}(96)$  is 5.4 km s $^{-1}$ . The dispersion around  $\vec{V}_{\text{flow}}(\text{He})$  of the 14 components best matching the LIC velocity (1.5 km s $^{-1}$ ) is only slightly better than the dispersion of these components about  $\vec{V}_{\text{flow}}(96)$  (1.6 km s $^{-1}$ ).

### 3.3. Regional Properties

The small filling factor of nearby ISM, combined with the component distribution, led to attempts to understand the positions of nearby ‘cloudlets’ (e.g. Lallement et al. 1986; Frisch 1996), the clouds towards  $\alpha$  Oph and  $\alpha$  Aql (Munch & Unsold 1962; Frisch 1981; Ferlet et al. 1986), and the “shape” of the cloud around the solar system (Frisch 1996; Redfield & Linsky 2000). These earlier approaches used velocities grouped either in the observed heliocentric velocity, or in the LIC velocity. Here we use an alternative approach, and evaluate cloud

membership in the rest frame of  $\vec{V}_{\text{flow}}(96)$ . Using the  $dV_i(96)$  values, we identify regional clumps of ISM based on similar  $dV_i(96)$  values for stars sampling a relatively compact region of the sky, except for the LIC which is identified by  $dV_i(\text{He})$  (or  $dV_i(20)$ ). The component groups that appear to represent subsets of the flow are listed in Table 4 and are discussed in order below. The positions of the clouds are plotted in Figure 6 as symbols overlying star positions.

### 3.3.1. 1. Cloud Surrounding the Solar System

The velocity of the interstellar cloud surrounding the solar system, the LIC, has been determined from observations of the resonance fluorescence of the 584 Å transition from interstellar  $\text{He}^{\circ}$  inside the solar system (e.g. Weller & Meier 1981; Flynn et al. 1998) and from *Ulysses in situ* measurements of interstellar  $\text{He}^{\circ}$  (Witte et al. 1996). Since the trajectories of interstellar H atoms inside the solar system are subject to radiation pressure, these  $\text{He}^{\circ}$  data yield the best LIC velocity. The *Ulysses GAS*-detector data give  $\vec{V}_{\text{flow}}(\text{He}) = -25.3 \pm 0.5$  km s<sup>-1</sup>,  $l^{\text{II}} = 3.9 \pm 1.0^{\circ}$ ,  $b^{\text{II}} = 15.8 \pm 1.3^{\circ}$  (and  $T = 6,550 \pm 1,050$  K) for the HC upstream direction (Witte et al. 1996, and private communication), which is within the uncertainties of the  $\text{He}^{\circ}$  584 Å backscattered radiation vector (Flynn et al. 1998). When this He motion is converted to a vector in the local standard of rest (LSR) using the *Hipparcos* solar apex motion (Dehnen & Binney 1998), the upstream direction corresponds to a velocity of  $-14.7$  km s<sup>-1</sup>, arriving from the upwind direction  $l^{\text{II}} = 345.9^{\circ}$ ,  $b^{\text{II}} = -1.1^{\circ}$ . In the LSR, this differs by  $\sim 2$  km s<sup>-1</sup> and  $\sim 20^{\circ}$  in direction from the bulk velocity vector. Pure deceleration of the flow would not alter the upstream direction, so shear motions may be present in the bulk flow.

*Copernicus*, *IUE* and *HubbleSpaceTelescope (HST)* observations of interstellar  $\text{D}^{\circ}$ ,  $\text{Fe}^+$ ,  $\text{Mg}^+$ , towards  $\alpha$  Cen (1.3 pc) indicate a HC velocity for the ISM in the range  $-17.7 \pm 0.1$  to  $-18.2 \pm 0.1$  km s<sup>-1</sup>, versus the value  $-16.1$  km s<sup>-1</sup> predicted by the projection of the *Ulysses* vector (Landsman et al. 1984; Lallement et al. 1995; Linsky & Wood 1996). This difference has been interpreted as indicating that the cloud surrounding the solar system terminates within  $\sim 10,000$  au of the Sun in the direction of  $\alpha$  Cen. The  $\alpha$  Cen cloud shows  $dV_i(\text{He}) \sim -2.8$  km s<sup>-1</sup> (and  $dV_i(96) = -3.8$  km s<sup>-1</sup>). This evidence for a cloud boundary close to the Sun in the direction of  $\alpha$  Cen is consistent with column densities measured towards the nearest stars, which indicate that  $<40\%$  of space is filled with ISM for volume density  $n(\text{H}^{\circ}) \sim 0.24$  cm<sup>-3</sup> as found for the LIC (SL02).

Thirty CLIC components have velocities consistent with the velocity of interstellar He inside the solar system ( $\vec{V}_{\text{flow}}(\text{He})$ ) using the criterion  $|dV_i(\text{He})| < 1.5$  km s<sup>-1</sup>. However,

components towards stars beyond 15 pc (Figure 1b) have predominantly negative  $dV_i(\text{He})$  values since these stars are generally located in the upstream direction. The stars showing these 30  $\vec{V}_{\text{flow}}(\text{He})$  components are distributed relatively uniformly across the sky (Figure 2d). Refitting the 30 components essentially reproduces  $\vec{V}_{\text{flow}}(\text{He})$ , and does not alter the distance dependence, suggesting the more distant components with  $|dV_i(\text{He})| < 1.5 \text{ km s}^{-1}$  either are blends of local and distant gas or are formed in independent cloudlets with no local contribution. The five stars within 15 pc with  $\vec{V}_{\text{flow}}(\text{He})$  components are  $\alpha \text{ CMa}$  (2.7 pc), 61 CygA (3.5 pc),  $\epsilon \text{ Ind}$  (3.6 pc), 40 EriA (5 pc), and  $\alpha \text{ Aur}$  (13 pc). The UV absorption lines towards  $\alpha \text{ CMi}$  (3.5 pc) have been fitted with both single-component and two-component models (Linsky et al. 1995). With the single-component fit (Table 3),  $dV_i(\text{He})=1.8 \text{ km s}^{-1}$ ; however  $dV_i(20)=0.5 \text{ km s}^{-1}$  so that  $\vec{V}_{\text{flow}}(20)$  provides a better fit for local gas towards this star. (A second component redshifted by  $\sim 2.6 \text{ km s}^{-1}$  (with  $\sim 50\%$  of the column density of the main component) is not coincident with either flow vector.)

The velocity vector of the cloud within the solar system provides poor agreement with the restricted sample of 96 components, as seen in Figure 3c where  $dV_i(\text{He})$  is plotted for all 96 components. The fact that  $|\vec{V}_{\text{flow}}(\text{He})| < |\vec{V}_{\text{flow}}(96)|$  yields the effect that nearby ISM in the downstream direction is blueshifted in the rest frame of  $\vec{V}_{\text{flow}}(96)$ .

Several studies have noted the small distance to the upstream cloud edge for the ISM surrounding the solar system ( $< 10^4 \text{ au}$ , e.g., LB92). The relative Sun-cloud velocity ( $\sim 25 \text{ pc}/10^6 \text{ yrs}$ ) suggests that the galactic environment of the Sun will vary within the next  $\sim 2,000$  years (Frisch 1997; Wood et al. 2000b).

The LIC is reliably identified only in the  $l^{\text{II}}=150^\circ \rightarrow 250^\circ$  interval where slightly more distant gas is absent, and in this interval  $\vec{V}_{\text{flow}}(\text{He})$  is an excellent descriptor of component velocities. The inability to identify the LIC reliably in sidestream and upstream directions indicates the two-flow model must be evaluated with caution in most sightlines, and in particular where velocity information is unavailable. In addition, since the CLIC represents a cluster of comoving clouds with a velocity dispersion of  $\sim 5 \text{ km s}^{-1}$ , simple closed surface LIC models which can be topologically deformed to a sphere may not realistically represent the LIC cloudlet.

### 3.3.2. Other Regional Component Groups

**2. Blue Cloud:** The “Blue Cloud” (BC) has been identified towards  $\alpha \text{ CMa}$  and  $\epsilon \text{ CMa}$ , placing the cloud within 3 pc of the Sun (Lallement et al. 1994; Hebrard et al. 1999; Gry & Jenkins 2001, GJ). The BC has  $dV_i(96) \sim -10 \text{ km s}^{-1}$ , and is blueshifted from the LIC by

$\sim 6.5 \text{ km s}^{-1}$ . The filling factor of the LIC towards  $\alpha$  CMa is  $f \sim 0.3$ , suggesting that the BC is a spatially separate feature. Towards  $\alpha$  CMa the BC appears to be cooler and denser than the LIC (Hebrard et al. 1999), while towards  $\epsilon$  CMa it appears warmer and denser than the LIC (GJ).

**3. Aquila-Ophiuchus Cloud:** The Aquila-Ophiuchus cloud (AOC) is disclosed by a set of  $\text{Ca}^+$  components with  $dV_i(96) = -6.1 \pm 0.9 \text{ km s}^{-1}$  towards stars located in the interval  $l^{\text{II}} = 28^\circ$  to  $48^\circ$ ,  $b^{\text{II}} = -5^\circ$  to  $+23^\circ$ . The stars  $\alpha$  Aql,  $\alpha$  Oph,  $\zeta$  Aql,  $\gamma$  Oph, and  $\lambda$  Aql show the Aql-Oph cloud component, and the 5.1 pc distance of  $\alpha$  Aql places the cloud close to the Sun. For each of these five background stars, the component formed in the AOC is the weakest and most blue-shifted component seen towards the star. The similarity between the AOC velocity and the velocity of weakest and most blueshifted component towards  $\delta$  Cyg ( $dV_i(96) = -6.9 \text{ km s}^{-1}$ ) may be a coincidence since the  $\delta$  Cyg component originates in a cold cloud ( $b = 0.47 \text{ km s}^{-1}$ ,  $0.42 \text{ km s}^{-1}$  for  $\text{Ca}^+$ ,  $\text{Na}^\circ$  respectively, Welty et al. 1996), and cold clouds are not expected within 5 pc. The AOC is located near the solar apex direction,  $l^{\text{II}} = 27.7^\circ$ ,  $b^{\text{II}} = 32.4^\circ$ . If the unobserved tangential velocity component is  $\sim 0 \text{ km s}^{-1}$ , the Sun may encounter this cloud within the next  $\sim 160,000$  years. Components from this cloud are seen clearly in Figure 3a.

**4. Pegasus-Aquarius Cloud:** The Pegasus-Aquarius cloud, with  $dV_i(96) = 4.2 \pm 0.5 \text{ km s}^{-1}$ , is seen towards stars grouped in the interval  $l^{\text{II}} = 75^\circ \pm 13^\circ$ ,  $b^{\text{II}} = -44^\circ \pm 5^\circ$ . Background stars are  $\theta$  Peg,  $\alpha$  Peg,  $\gamma$  Aqr,  $\eta$  Aqr, and this cloud must be within 30 pc of the Sun.

**5. North Pole Cloud:** A group of components with velocity  $1.7 \pm 0.6 \text{ km s}^{-1}$  is found towards stars at high galactic latitudes,  $b^{\text{II}} > 53^\circ$ , including the Ursa Majoris region. The nearest star with a component in this group is  $\alpha$  CrB, at 23 pc.

**6. South Pole Cloud:** A cloud with  $\vec{V}_{\text{flow}}(96) = 2.4 \pm 1.0 \text{ km s}^{-1}$  occupies an irregularly shaped region covering the South Galactic Pole ( $b^{\text{II}} \leq 48^\circ$ ). The South Pole Cloud (SPC) cloud is seen towards  $\epsilon$  Ind,  $\alpha$  Hyi,  $\tau^3$  Eri,  $\beta$  Cet. However, two of these components (towards  $\epsilon$  Ind and  $\beta$  Cet) also have  $|dV_i(\text{He})| < 0.1 \text{ km s}^{-1}$ , indicating they also could be formed in the LIC (which is seen towards two other low latitude stars, 40 Eri and EP Eri). If so, the SPC is not a separate cloudlet. The nearest star in this sample is  $\epsilon$  Ind at 3.6 pc, indicating the SPC, if real, is quite nearby. Additional data are required to test for the SPC.

**7. Filamentary-like Feature:** Perhaps the most puzzling of the component groups suggests a filamentary structure, with  $dV_i(96) = +6.9 \pm 1.5 \text{ km s}^{-1}$ . Since this feature has a large angular extent ( $\sim 90^\circ$ , Figure 6), it represents a single cloudlet only if the tangential (unobserved) velocity is  $\sim 0 \text{ km s}^{-1}$  for all of the stars, similar to a fragment of an expanding ring. This feature is at  $l^{\text{II}} = 284^\circ \pm 12^\circ$ ,  $b^{\text{II}} = -4^\circ \pm 50^\circ$ , and it is seen towards  $\delta \text{ CrV}$ ,  $\gamma \text{ CrV}$ , HR 4023,  $\delta \text{ Vel}$ ,  $\alpha \text{ Hyi}$ . Four additional stars ( $61 \text{ Cyg}$ ,  $\beta \text{ Cet}$ ,  $\alpha \text{ And}$ ,  $\beta \text{ Ser}$ ) also show a component at this velocity, which would be related to the filament *only* if the expansion interpretation is correct.

#### 4. Conclusions

The principal conclusions of this paper are that:

1. The bulk flow velocity for interstellar matter within  $\sim 30 \text{ pc}$  of the Sun is determined from optical and UV absorption line data. A self-consistent flow vector is determined if stars with infrared-emitting circumstellar disks ( $\epsilon \text{ Eri}$ ,  $\beta \text{ Pic}$ ,  $\beta \text{ Leo}$ ,  $\alpha \text{ Lyr}$ , and  $\alpha \text{ PsA}$ ), variable emission lines ( $\alpha \text{ Eri}$ ), and HR 1099 are omitted from the sample. Fits to the remaining 96 component sample (60 stars) yield a bulk flow velocity ( $\vec{V}_{\text{flow}}(96)$ ) through the LSR (using *Hipparcos* data on the solar apex motion) of magnitude  $-17.0 \text{ km s}^{-1}$ , with an upstream direction of  $l^{\text{II}} = 2.3^\circ$ ,  $b^{\text{II}} = -5.2^\circ$  (Table 1). In the heliocentric velocity frame (i.e. with respect to the Sun),  $|\vec{V}_{\text{flow}}(96)| = -28.1 \text{ km s}^{-1}$ , arriving from the direction  $l^{\text{II}} = 12.4^\circ$ ,  $b^{\text{II}} = +11.6^\circ$  (the  $1\text{-}\sigma$  velocity uncertainty is  $\pm 4.6 \text{ km s}^{-1}$ , based on the component distribution about the bulk flow velocity).

2. The CLIC gas (Cluster of Local Interstellar Clouds) is defined by this ensemble of velocity components, which show a Gaussian or exponential distribution in the rest frame of the central flow velocity, and the dispersion of this distribution is typical for dispersions determined from lower resolution observations of diffuse clouds. The dispersion in the velocities of the individual CLIC components partaking in the bulk flow explains the difference between the velocity of the interstellar cloud inside the solar system ( $25.3 \text{ km s}^{-1}$ , HC) versus the overall bulk flow velocity ( $-28.1 \text{ km s}^{-1}$ , HC).

3. This LSR upstream direction suggests the CLIC gas may be part of a superbubble shell expanding from the Loop I supernova remnant, or from an earlier epoch of superbubble formation in the Scorpius-Centaurus Association. The cold absorption component formed in the polar cap of Loop I appears to be present in front of  $\alpha \text{ Pav}$ .

4. The velocity of the interstellar cloud observed inside the solar system, and in the downstream direction towards nearby stars ( $\vec{V}_{\text{flow}}(\text{He})$ ) differs both from  $\vec{V}_{\text{flow}}(96)$ , and from

the velocity of ISM towards the nearest star  $\alpha$  Cen. However, 85% of the observed components consistent with  $\vec{V}_{\text{flow}}(\text{He})$  are probably formed in unrelated parts of the CLIC. This complexity suggests that simple smooth closed-surface models for local interstellar gas are unlikely to be accurate in detail. The components within  $1.5 \text{ km s}^{-1}$  of the velocity of interstellar He within the solar system ( $\vec{V}_{\text{flow}}(\text{He})$ ) dominate the galactic longitude interval  $l^{\text{II}}=150^{\circ}\rightarrow 250^{\circ}$ , suggesting a deceleration of the flow in the third galactic quadrant. The Sun is likely to emerge from the gas-patch now surrounding it within the next several thousand years.

5. Several spatially distinct groups of components sharing a common  $dV_i(96)$  suggest the bulk flow is composed of cloudlets (Table 4), including the previously known LIC and Blue Cloud in the downstream direction. Distinct cloudlets in the upstream direction include the Aquila-Ophiuchus cloud with components at  $dV_i(96)\sim -6 \text{ km s}^{-1}$ . This cloud may extend to within 5 pc of the Sun since it is seen towards  $\alpha$  Aql. Components in this cloud form the weakest and highest velocity  $\text{Ca}^+$  component for each star in which it is observed. This cloud is in the solar apex direction, and if the non-radial component of the cloud velocity is small the Sun will encounter this cloud in  $<200,000$  years. A distinct cloud is seen towards Pegasus/Aquarius, at  $dV_i(96)=3.8\pm 0.3 \text{ km s}^{-1}$ . Another distinct cloud is found within 22 pc towards the North Galactic Pole, with  $dV_i(96)=1.7\pm 0.6 \text{ km s}^{-1}$ .

6. These results show the kinematics of CLIC components are consistent with early studies showing macroscopic turbulence in the ISM within  $\sim 500$  pc (Blaauw 1952; Münch 1957). Low filling factors for nearby ISM ( $<40\%$ ), and mean cloudlet speed  $\eta \sim 5 \text{ km s}^{-1}$  in the flow reference frame ( $\vec{V}_{\text{flow}}(96)$ ) suggest that the CLIC is a cluster of comoving cloudlets. If this velocity dispersion is due to turbulence (as the larger samples considered by Blaauw and Münch suggest), then it is distinct from the microscopic turbulence which broadens absorption lines towards nearby stars ( $b^2=2kT/m + 2V_{\text{turb}}^2$ , where  $V_{\text{turb}} \sim 1 \text{ km s}^{-1}$ ).

7. A two-flow model of the velocity components is not a unique description of CLIC gas. For example, the velocity dispersion of  $\vec{V}_{\text{flow}}(76)$  is about equal to the difference between the  $\vec{V}_{\text{flow}}(76)$  and  $\vec{V}_{\text{flow}}(20)$  velocities ( $\sim 4 \text{ km s}^{-1}$ ). In addition, multiple components in the downstream gas are not accommodated by a two-flow model. The result is that morphological models of the LIC must include velocity information for accurate results.

Studies of the CLIC, where individual cloudlets can be studied in high resolution UV data, and in some sightlines in optical data, offer the best opportunity for reliably determining the relation between the kinematical and spatial characteristics of diffuse interstellar clouds.

This research has been supported by NASA grants NAG5-6405 (Frisch), NAG5-8163

(Frisch), and NAG5-3228 (Welty).

## REFERENCES

- Adams, T. F. & Frisch, P. C. 1977, *ApJ*, 212, 300
- Adams, W. S. 1949, *ApJ*, 109, 354
- Berkhuijsen, E. M. 1971, *A&A*, 14, 359
- . 1973, *A&A*, 24, 143
- Bertin, P., Lallement, R., Ferlet, R., & Vidal-Madjar, A. 1993, *J. Geophys. Res.*, 98, 15193
- Blaauw, A. 1952, *Bull. Astron. Inst. Netherlands*, 11, 459
- Bruhweiler, F. C. & Kondo, Y. 1982, *ApJ*, 259, 232
- Crawford, I. A. 1991, *A&A*, 247, 183
- Crawford, I. A., Craig, N., & Welsh, B. Y. 1997, *A&A*, 317, 889
- Crawford, I. A. & Dunkin, S. K. 1995, *MNRAS*, 273, 219
- Crawford, I. A., Lallement, R., & Welsh, B. Y. 1998, *MNRAS*, 300, 1181
- Crutcher, R. M. 1982, *ApJ*, 254, 82
- de Geus, E. J. 1992, *A&A*, 262, 258
- Dehnen, W. & Binney, J. J. 1998, *MNRAS*, 298, 387
- Dring, A. R., Linsky, J., Murthy, J., Henry, R. C., Moos, W., Vidal-Madjar, A., Audouze, J., & Landsman, W. 1997, *ApJ*, 488, 760
- Ferlet, R., Lecavelier Des Etangs, A., Vidal-Madjar, A., Bertin, P., Deleuil, M., Lagrange-Henri, A. ., & Lallement, R. 1995, *A&A*, 297, L5
- Ferlet, R., Vidal-Madjar, A., & Lallement, R. 1986, *A&A*, 163, 204
- Flynn, B., Vallergera, J., Dalaudier, F., & Gladstone, G. R. 1998, *J. Geophys. Res.*, 103, 6483
- Frisch, P. & York, D. G. 1986, in *The Galaxy and the Solar System* (University of Arizona Press), 83–100

- Frisch, P. C. 1979, *ApJ*, 227, 474
- . 1981, *Nature*, 293, 377
- . 1986, *Adv. Space Res.*, 6, 345
- . 1993, *ApJ*, 407, 198
- . 1995, *Space Sci. Rev.*, 72, 499
- . 1996, *Space Sci. Rev.*, 78, 213
- Frisch, P. C. 1997, <http://xxx.lanl.gov/>, astro-ph/9705231
- Frisch, P. C. 2001, in XVIIth IAP Conference: Gaseous Matter in Galaxies and Intergalactic Space, in press
- Frisch, P. C., Dorschner, J. M., Geiss, J., Greenberg, J. M., Grün, E., Landgraf, M., Hoppe, P., Jones, A. P., Krätschmer, W., Linde, T. J., Morfill, G. E., Reach, W., Slavin, J. D., Svestka, J., Witt, A. N., & Zank, G. P. 1999, *ApJ*, 525, 492
- Frisch, P. C. & Welty, D. E. 2002, In preparation
- Frisch, P. C. & York, D. G. 1983, *ApJ*, 271, L59
- Gayley, K. G., Zank, G. P., Pauls, H. L., Frisch, P. C., & Welty, D. E. 1997, *ApJ*, 487, 259
- Gry, C. & Jenkins, E. B. 2001, *A&A*, 367, 617
- Habing, H. J., Dominik, C., Jourdain de Muizon, M., Laureijs, R. J., Kessler, M. F., Leech, K., Metcalfe, L., Salama, A., Siebenmorgen, R., Trams, N., & Bouchet, P. 2001, *A&A*, 365, 545
- Hartmann, D. & Burton, W. B. 1997, *Atlas of Galactic Neutral Hydrogen* (Cambridge: Cambridge University Press)
- Haslam, C. G. T., Stoffel, H., Salter, C. J., & Wilson, W. E. 1982, *A&AS*, 47, 1
- Hebrard, G., Mallouris, C., Ferlet, R., Koester, D., Lemoine, M., Vidal-Madjar, A., & York, D. 1999, *A&A*, 350, 643
- Heiles, C. 1989, *ApJ*, 336, 808
- . 1998, *ApJ*, 498, 689

- Hobbs, L. M., Ferlet, R., Welty, D. E., & Wallerstein, G. 1991, *ApJ*, 378, 586
- Lallement, R. & Bertin, P. 1992, *A&A*, 266, 479
- Lallement, R., Bertin, P., Ferlet, R., Vidal-Madjar, A., & Bertaux, J. L. 1994, *A&A*, 286, 898
- Lallement, R., Ferlet, R., Lagrange, A. M., Lemoine, M., & Vidal-Madjar, A. 1995, *A&A*, 304, 461
- Lallement, R., Vidal-Madjar, A., & Ferlet, R. 1986, *A&A*, 168, 225
- Landsman, W. B., Henry, R. C., Moos, H. W., & Linsky, J. L. 1984, *ApJ*, 285, 801
- Linsky, J. L., Diplas, A., Wood, B. E., Brown, A., Ayres, T. R., & Savage, B. D. 1995, *ApJ*, 451, 335
- Linsky, J. L. & Wood, B. E. 1996, *ApJ*, 463, 254
- McClintock, W., Henry, R. C., Linsky, J. L., & Moos, H. W. 1978, *ApJ*, 225, 465
- Münch, G. 1957, *ApJ*, 125, 42
- Munch, G. & Unsold, A. 1962, *ApJ*, 135, 711
- Piskunov, N., Wood, B. E., Linsky, J. L., Dempsey, R. C., & Ayres, T. R. 1997, *ApJ*, 474, 315
- Porri, A. & Stalio, R. 1988, *A&AS*, 75, 371
- Redfield, S. & Linsky, J. L. 2000, *ApJ*, 534, 825
- Sahu, M. S., Landsman, W., Bruhweiler, F. C., Gull, T. R., Bowers, C. A., Lindler, D., Feggans, K., Barstow, M. A., Hubeny, I., & Holberg, J. B. 1999, *ApJ*, 523, L159
- Slavin, J. D. & Frisch, P. C. 2002, *ApJ*, 565, 364
- Spitzer, L. J. 1942, *ApJ*, 95, 329
- Vallerga, J. V., Vedder, P. W., Craig, N., & Welsh, B. Y. 1993, *ApJ*, 411, 729
- Weller, C. S. & Meier, R. R. 1981, *ApJ*, 246, 386
- Welty, D. E., Morton, D. C., & Hobbs, L. M. 1996, *ApJS*, 106, 533
- Witte, M., Banaszekiewicz, M., & Rosenbauer, H. 1996, *Space Sci. Rev.*, 78, 289

Wood, B. & Linsky, J. 1998, ApJ, 492, 788

Wood, B. E., Alexander, W. R., & Linsky, J. L. 1996a, ApJ, 470, 1157

Wood, B. E., Ambruster, C. W., Brown, A., & Linsky, J. L. 2000a, ApJ, 542, 411

Wood, B. E., Harper, G. M., Linsky, J. L., & Dempsey, R. C. 1996b, ApJ, 458, 761

Wood, B. E., Linsky, J. L., & Zank, G. P. 2000b, ApJ, 537, 304

Zank, G. P. & Frisch, P. C. 1999, ApJ, 518, 965

Table 1. Streaming Motions in HC and LSR Rest Frames

	HC Vector <sup>a</sup>			LSR Vector <sup>a,b</sup>			Sample <sup>c</sup>
	Vel. km s <sup>-1</sup>	l Deg.	b Deg.	Vel. km s <sup>-1</sup>	l Deg.	b Deg.	
Bulk Fits:							
$\vec{V}_{\text{flow}}(96)$	-28.1±4.6	12.4	11.6	-17.0	2.3	-5.2	60 stars
$\vec{V}_{\text{flow}}(46)$	-28.1±4.3	12.5	12.5				31 stars, d<29 pc
Upstream:							
$\vec{V}_{\text{flow}}(76)$	-29.3±4.0	13.1	11.2	-18.1	3.9	-4.7	46 stars
$\vec{V}_{\text{flow}}(\text{G})$	-29.4	4.5	20.5				G-cloud (Lallement & Bertin 1992)
Downstream, $l^{\text{II}}=150\rightarrow 250$ :							
$\vec{V}_{\text{flow}}(\text{He})$	-25.3±0.5	3.9±1.0	15.8±1.3	-14.7	345.9	-1.1	<i>Ulysses</i> He <sup>o</sup> value (Witte et al. 1996)
$\vec{V}_{\text{flow}}(20)^{\text{d}}$	-25.8±4.3	6.2	10.4				14 stars
$\vec{V}_{\text{flow}}(584\text{\AA})$	-26.4±1.5	4.5±0.6	14.2±0.6				Backscattered He <sup>o</sup> 584 Å (Flynn et al. 1998)

<sup>a</sup>Galactic coordinates correspond to upstream directions. The velocity uncertainty is the 1- $\sigma$  value of the component distribution about the bulk flow velocity.

<sup>b</sup>Based on Hipparcos solar apex motion (Dehnen & Binney 1998).

<sup>c</sup>Sample stars are listed in Tables 2 and 3.

<sup>d</sup>The dispersion of the same 14 components around  $\vec{V}_{\text{flow}}(\text{He})$  is  $\pm 1.7$  km s<sup>-1</sup>.

Table 2. Data Sources

Reference	Nominal Resl. <sup>a</sup> km s <sup>-1</sup>	Star List
Optical Data:		
Frisch & Welty (2002, FW02)	1.3–1.5	$\alpha$ CMa, $\alpha$ Leo, $\eta$ UMa, $\gamma$ UMa, $\delta$ UMa, $\beta$ Lib $\alpha$ CrB, $\lambda$ Oph, $\delta$ Her, $\nu$ Ser, $\beta$ Ser, $o$ Ser, $\lambda$ Aql $\zeta$ Aql, $\alpha$ Aql, $\beta$ Aur, $\alpha$ Peg
Crawford et al. (1998, CLW98)	0.35	$\alpha$ And, $\delta$ Vel, $\alpha$ Pav, $\theta$ Peg
Crawford et al. (1997, CCW97)	0.35	$\alpha$ Hyi, $\iota$ Cen, $\epsilon$ Gru, $\gamma$ Aqr, $\gamma$ Oph
Welty et al. (1996, W96)	1.2	$\gamma$ CrV, $\delta$ CrV, $\delta$ Cyg
Crawford & Dunkin (1995, CD95)	0.3	$\alpha$ Oph, $\alpha$ Gru, $\alpha$ Eri
Vallerga et al. (1993, V93)	1.9	$\alpha 2$ CVn, $\eta$ Aqr, $\kappa$ And
Bertin et al. (1993, B93)	3.0	$\tau 3$ Eri, HR 4023
Lallement & Bertin (1992, LB92)	3.0	$\alpha$ Cep, $\delta$ Cas, $\alpha$ Lac
Ultraviolet Data:		
Gry & Jenkins (2001, GJ01)	2.7	$\epsilon$ CMa
Wood et al. (2000b, WLZ00)	2.7	36 Oph
Wood et al. (2000a, W00)	~15	EP Eri, DX Leo, LQ Hya, V368 Cep
Sahu et al. (1999, Sa99)	2.7	G191-B2B
Hebrard et al. (1999, H99)	2.7	$\alpha$ CMa
Wood & Linsky (1998, WL98)	3.5	61 Cyg, 40 Eri A
Dring et al. (1997, D97)	3.5	$\epsilon$ Eri, $\beta$ Gem, $\alpha$ Tri, $\sigma$ Gem, 31 Com
Wood et al. (1996a, WAL96)	3.5	$\epsilon$ Ind, $\lambda$ And
Piskunov et al. (1997, P97)	3.5	$\beta$ Cet
Ferlet et al. (1995, Fer95)	3.5	$\alpha$ PsA
Linsky et al. (1995, Lin95)	3.5	$\alpha$ CMi, $\alpha$ Aur
Lallement et al. (1995, Lal95)	3.5	$\alpha$ Lyr, $\beta$ Leo, $\beta$ Pic

Table 3. Velocity Components of Unrestricted Sample

HD	Name	l deg.	b deg.	d pc	Spec.	N(X) <sup>a</sup>	Velocity km s <sup>-1</sup>	dV <sub>i</sub> (96) km s <sup>-1</sup>	Ref. <sup>b</sup>
128621	$\alpha$ CenB	315.7	-0.7	1.4	G1pl	3.89e17	-18.9	-3.8	P97
48915	$\alpha$ CMa	227.2	-8.9	2.6	A1V	2.5e17	13.7	-9.5	H99
						0.16e10	19.6	-3.6	FW02
22049 <sup>c,d</sup>	$\epsilon$ Eri	196.	-48.	3.2	K2V	7.50e17	21.3	-1.3	D97
61421	$\alpha$ CMi	213.7	13.0	3.5	F5IV/V	7.59e17	20.8	-3.0	Lin95
201092	61 CygA	82.	-6.	3.5	K5V	7.08e17	-9.0	0.0	WL98
						7.41e17	-3.0	6.0	WL98
209100	$\epsilon$ Ind	336.2	-48.0	3.6	K4.5V	1.00e18	-9.2	1.5	WAL96
26965	40 EriA	201.	-38.	5.0	K1V	8.71e17	21.6	-3.4	WL98
155886	36 OphAB	358.30	6.88	5.	K1V/K0V	7.08e17	-28.4	-1.2	WZ
187642	$\alpha$ Aql	47.7	-8.9	5.1	A7V	0.3e10	-26.9	-5.5	FW02
						0.5e10	-22.8	-1.4	FW02
						0.9e10	-18.1	3.3	FW02
172167 <sup>c,d</sup>	$\alpha$ Lyr	67.5	19.2	7.6	A0V	6.5e12	-18.3	-1.5	Lal95
						6.9e12	-16.0	0.8	Lal95
						1.03e13	-12.7	4.1	Lal95
216956 <sup>c,d</sup>	$\alpha$ PsA	20.5	-64.9	7.7	A3V	3.8e12	-3.2	3.3	Fer95
						1.8e12	-9.7	-3.2	Fer95
17925	EP Eri	192.07	-58.25	10.4	K2V	8.9e17	19.	-0.3	W00
62509	$\beta$ Gem	192.2	23.4	10.6	K0II	1.15e18	21.9	-1.2	D97
						6.82e17	33.0	9.9	D97
102647 <sup>c,d</sup>	$\beta$ Leo	250.6	70.8	11.0	A3V	...	-0.8	-0.3	Lal95
						...	2.7	3.2	Lal95
						...	13.3	13.8	Lal95
34029	$\alpha$ Aur	162.6	4.6	12.9	G5IIIepI	1.74e18	22.0	-1.4	Lin95
159561	$\alpha$ Oph	35.9	22.6	14.3	A5III	1.00e11	-23.6	1.9	CD95
						1.58e11	-26.2	-0.7	CD95
						1.59e10	-32.0	-6.5	CD95
						6.31e10	-28.4	-2.9	CD95
203280	$\alpha$ Cep	101.0	9.2	15.0	A7IV	0.7e10	0.2	1.8	LB92
432	$\beta$ Cas	117.5	-3.3	16.7	F2IV	1.51e18	10	2.5	P97

Table 3—Continued

HD	Name	l deg.	b deg.	d pc	Spec.	N(X) <sup>a</sup>	Velocity km s <sup>-1</sup>	dV <sub>i</sub> (96) km s <sup>-1</sup>	Ref. <sup>b</sup>
11443	$\alpha$ Tri	138.6	-31.4	17.5	F6IV	1.15e18	17.6	0.8	D97
						9.79e17	12.7	-4.1	D97
82443	DX Leo	201.21	46.06	17.7	K2V	5.e17	11.	-3.8	W00
115892	$\iota$ Cen	309.4	25.8	18.0	A2V	2.5e10	-18.2	-4.5	CCW97
82558	LQ Hya	244.59	28.40	18.3	K2V	5.62e18	6.	-6.2	W00
39060 <sup>c,d</sup>	$\beta$ Pic	258.4	-30.6	19.3	A5V	...	-3.2	-15.7	Fer95
						...	-9.7	-22.2	Fer95
220140	V368Cep	118.46	16.94	19.7	K2V	8.9e17	5.	-0.6	W00
12311	$\alpha$ Hyi	289.5	-53.8	21.9	F0V	2.88e10	9.8	7.3	CCW97
						5.01e10	4.9	2.4	CCW97
139006	$\alpha$ CrB	41.9	53.8	22.9	A0V	1.03e10	-17.4	1.3	FW02
87901	$\alpha$ Leo	226.4	48.9	23.8	B7V	0.5e10	10.5	-0.3	FW02
156164	$\delta$ Her	46.8	31.4	24.1	A3IV	3.1e10	-19.7	2.7	FW02
74956	$\delta$ Vel	272.1	-7.4	24.4	A1V	0.86e10	15.6	10.0	CLW98
						2.38e10	1.3	-4.3	CLW98
						4.34e10	11.6	6.0	CLW98
106591	$\delta$ UMa	132.6	59.4	25.0	A3V	0.9e10	3.8	1.6	FW02
40183	$\beta$ Aur	167.5	10.4	25.2	A2IVpl	1.0e10	22.3	-1.3	FW02
177724	$\zeta$ Aql	46.9	3.3	25.5	A0Vn	0.6e10	-24.5	-1.5	FW02
						0.9e10	-20.6	2.4	FW02
						1.4e10	-29.7	-6.7	FW02
103287	$\gamma$ UMa	140.7	61.4	25.6	A0V	0.8e10	4.4	1.2	FW02
222107	$\lambda$ And	109.9	-14.5	25.8	G8III	2.81e18	6.5	1.6	WAL96
18978	$\tau$ 3 Eri	213.5	-60.3	26.4	A4V	2.0e10	15.9	-1.7	B93
						3.0e10	20.9	3.3	B93
108767	$\delta$ CrV	295.5	46.1	26.9	B9.5V	3.4e10	-0.5	7.9	W96
22468	HR 1099	184.9	-41.6	29.0	G5IV/K1IV	7.9e17	21.9	-2.3	P97
						1.6e17	8.2	-16.0	P97
						4.0e17	14.8	-9.4	P97
161868	$\gamma$ Oph	28.0	15.0	29.1	A0V	3.0e10	-33.1	-6.0	CCW97
						4.2e10	-29.9	-2.8	CCW97

Table 3—Continued

HD	Name	l deg.	b deg.	d pc	Spec.	N(X) <sup>a</sup>	Velocity km s <sup>-1</sup>	dV <sub>i</sub> (96) km s <sup>-1</sup>	Ref. <sup>b</sup>
4128	$\beta$ Cet	111.3	-80.7	29.4	K0III	5.9e16	1.	-5.3	P97
						2.23e18	8.	1.7	P97
120418	$\theta$ Peg	67.4	-38.7	29.6	A2IV	3.0e10	-4.2	4.6	CLW98
358	$\alpha$ And	111.7	-32.8	29.8	B8IVp	1.99e10	13.0	6.2	CLW98
8538	$\delta$ Cas	127.2	-2.4	30.5	A5III-IV	0.51e10	12.9	1.1	LB92
120315	$\eta$ UMa	100.7	65.3	30.9	B3V	0.9e10	-3.4	2.1	FW02
209952 <sup>c</sup>	$\alpha$ Gru	350.0	-52.4	31.1	B7IV	2.0e10	13.0	-1.9	CD95
						1.12e10	10.2	0.9	CD95
213558	$\alpha$ Lac	101.3	-6.6	31.4	A1V	1.0e10	3.5	3.4	LB92
88955	HR 4023	274.3	11.9	31.5	A2V	2.38e10	-1.7	-4.4	CLW98
						3.98e10	10.5	7.8	CLW98
112413	$\alpha$ 2 CVn	118.3	78.8	33.8	A0spe	0.51e10	-1.9	2.2	V93
177756	$\lambda$ Aql	30.3	-5.5	38.4	B9Vn	0.41e10	-21.9	3.7	FW02
						0.41e10	-26.5	-0.9	FW02
						0.96e10	-30.7	-5.1	FW02
215789	$\epsilon$ Gru	338.3	-56.5	39.7	A3V	1.58e10	-12.2	-4.3	CCW97
						1.95e10	-7.2	0.7	CCW97
						2.88e10	-1.1	6.8	CCW97
218045	$\alpha$ Peg	88.3	-40.4	42.8	B9III	0.8e10	-4.7	-3.2	FW02
						1.1e10	-0.5	1.0	FW02
						0.6e10	2.5	4.0	FW02
10144 <sup>c,e</sup>	$\alpha$ Eri	290.8	-58.8	44.0	B3Vpe	0.50e10	18.9	16.2	CD95
						1.26e10	21.2	18.5	CD95
						1.86e10	11.0	8.3	CD95
						2.51e10	7.6	4.9	CD95
141003	$\beta$ Ser	26.0	47.9	46.9	A2IV	1.0e10	-16.7	5.5	FW02
						2.9e10	-23.3	-1.1	FW02
						6.6e10	-20.7	1.5	FW02
212061	$\gamma$ Aqr	62.2	-45.8	48.4	A0V	7.94e9	-4.5	3.9	CCW97
135742	$\beta$ Lib	352.0	39.2	49.1	B8V	0.8e10	-33.7	-10.1	FW02
						6.4e10	-23.6	0.0	FW02

Table 3—Continued

HD	Name	l deg.	b deg.	d pc	Spec.	N(X) <sup>a</sup>	Velocity km s <sup>-1</sup>	dV <sub>i</sub> (96) km s <sup>-1</sup>	Ref. <sup>b</sup>
						6.4e10	-26.9	-3.3	FW02
106625	$\gamma$ CrV	291.0	44.5	50.0	B8IIIp	1.5e10	1.6	8.5	W96
						5.4e10	-2.0	4.9	W96
148857	$\lambda$ Oph	17.1	31.8	50.9	A0Vpl	4.7e10	-24.8	1.5	FW02
160613	$o$ Ser	13.3	9.2	51.5	A2Va	5.6e10	-29.0	-0.9	FW02
222439	$\kappa$ And	109.8	-16.7	52.0	B9IVn	1.1e10	0.8	-4.2	V93
						6.1e10	7.6	2.6	V93
186882	$\delta$ Cyg	78.7	10.2	52.4	B9.5IV	2.8e10	-18.8	-6.9	W96
						2.9e10	-16.3	-4.4	W96
						3.2e10	-9.6	2.3	W96
62044	$\sigma$ Gem	191.2	23.3	55.5	K1III	5.85e17	32.0	8.9	D97
						7.50e17	21.4	-1.7	D97
193924	$\alpha$ Pav	340.9	-32.5	56.2	B2IV	1.24e10	-19.6	-2.8	CLW98
						1.05e11	-18.6	-1.8	CLW98
213998	$\eta$ Aqr	66.8	-47.6	56.3	B9IV-Vn	2.70e10	-2.1	4.6	V93
156928	$\nu$ Ser	10.6	13.5	59.3	A0/A1V	4.4e10	-27.7	0.4	FW02
WD0501+527	G191-B2B	155.95	+7.1	68.82	DAw	1.86e18	19.3	-2.0	Sa99
						3.98e17	8.6	-12.7	Sa99
111812	31 Com	114.9	89.6	90.9	G0II	7.66e17	-2.4	3.2	D97
52089	$\epsilon$ CMa	239.8	-11.3	132.	A1V	4.0e17	9.2	-10.2	GJ01 <sup>f</sup>
						6.0e17	16.2	-3.2	GJ01

<sup>a</sup>Column Densities less than  $10^{13}$  are for  $\text{Ca}^+$ , and values greater than this are based on  $N(\text{H}^{\circ})$  measurements.

<sup>b</sup>References are listed in Table 2.

<sup>c</sup>Star omitted from restricted sample used for determining  $\vec{V}_{\text{flow}}(93)$ , see text.

<sup>d</sup> $\alpha$  Eri is the brightest known Be emission line star, with evidence of variable chromosphere and variable stellar radial velocities (Porri & Stalio 1988).

<sup>e</sup>Star with infrared excess indicating dust disk (e.g. Habing et al. 2001).

<sup>f</sup>Velocities are from GJ01 text and not GJ01 table.

Table 4. Regional Properties of Flow

Cloud <sup>a</sup> Name	Vector	dV <sub>i</sub> Range (km s <sup>-1</sup> )	Location <sup>b</sup> $d_{\min}, l^{\text{II}}, b^{\text{II}}$	Stars Showing Cloud Component
1 LIC	$\vec{V}_{\text{flow}}(\text{He})$	0.0±1.5	0 pc, $l^{\text{II}}=150^{\circ}\rightarrow 250^{\circ}$	All stars in interval
2 <sup>c</sup> Blue Cloud	$\vec{V}_{\text{flow}}(96)$	-9.8±0.3	<3 pc, $233^{\circ}\pm 7^{\circ}, 10^{\circ}\pm 2^{\circ}$	$\alpha$ CMa, $\epsilon$ CMa
3 Aql/Oph	$\vec{V}_{\text{flow}}(96)$	-6.1±1.0	<5 pc, $38^{\circ}\pm 10^{\circ}, 9^{\circ}\pm 14^{\circ}$	$\alpha$ Aql, $\alpha$ Oph, $\zeta$ Aql, $\gamma$ Oph, $\lambda$ Aql ( $\delta$ Cyg)
4 Peg/Aqr	$\vec{V}_{\text{flow}}(96)$	4.2±0.5	<30 pc, $75^{\circ}\pm 13^{\circ}, -44^{\circ}\pm 5^{\circ}$	$\theta$ Peg, $\alpha$ Peg, $\gamma$ Aqr, $\eta$ Aqr
5 North Pole	$\vec{V}_{\text{flow}}(96)$	1.7±0.6	<22 pc, $b^{\text{II}}>+47^{\circ}$ ,	$\gamma$ UMa, $\alpha$ CrB, $\delta$ UMa, $\eta$ UMa, $\alpha^2$ CVn, $\beta$ Ser
6 South Pole:	$\vec{V}_{\text{flow}}(96)$	2.4±1.0	<3.6 pc, $b^{\text{II}}\leq-48^{\circ}$	$\epsilon$ Ind, $\alpha$ Hyi, $\tau^3$ Eri, $\beta$ Cet
7 Filament:	$\vec{V}_{\text{flow}}(96)$	6.7±1.8	<22 pc, $284^{\circ}\pm 12^{\circ}, -4^{\circ}\pm 50^{\circ}$	$\delta$ CrV, $\gamma$ CrV, HR4023, $\delta$ Vel, $\alpha$ Hyi, $\epsilon$ Gru

<sup>a</sup>Clouds marked with a “:” are poorly identified and uncertain.

<sup>b</sup> $d_{\min}$  is the minimum cloud distance.

<sup>c</sup>Cloud 2 is the “Blue Cloud” (Lallement et al. 1994; Gry & Jenkins 2001).

Table 5. LISM Heliocentric Velocity Vectors

Vector	V km s <sup>-1</sup>	l °	b °	Basis	Ref.
Crutcher (C)	-28±2	25	+10	Optical Ti <sup>+</sup> , d<100 pc stars	Crutcher (1982)
Frisch & York (FY)	-27	34	+15	Optical Ca <sup>+</sup> , d<100 pc stars	Frisch & York (1986)
LIC	26±1	6±3	16±3	Ca <sup>+</sup>	LB92, Bertin et al. (1993)
G	29	4.5	20.5	Ca <sup>+</sup>	Bertin et al. (1993)
Frisch (F)	-26.8±1.3	6.2	11.7	Ca <sup>+</sup> , d<50 pc stars	Frisch (1995)
Bulk Flow (BF)	-28.1±4.6	12.4	11.6	UV, Optical	This work

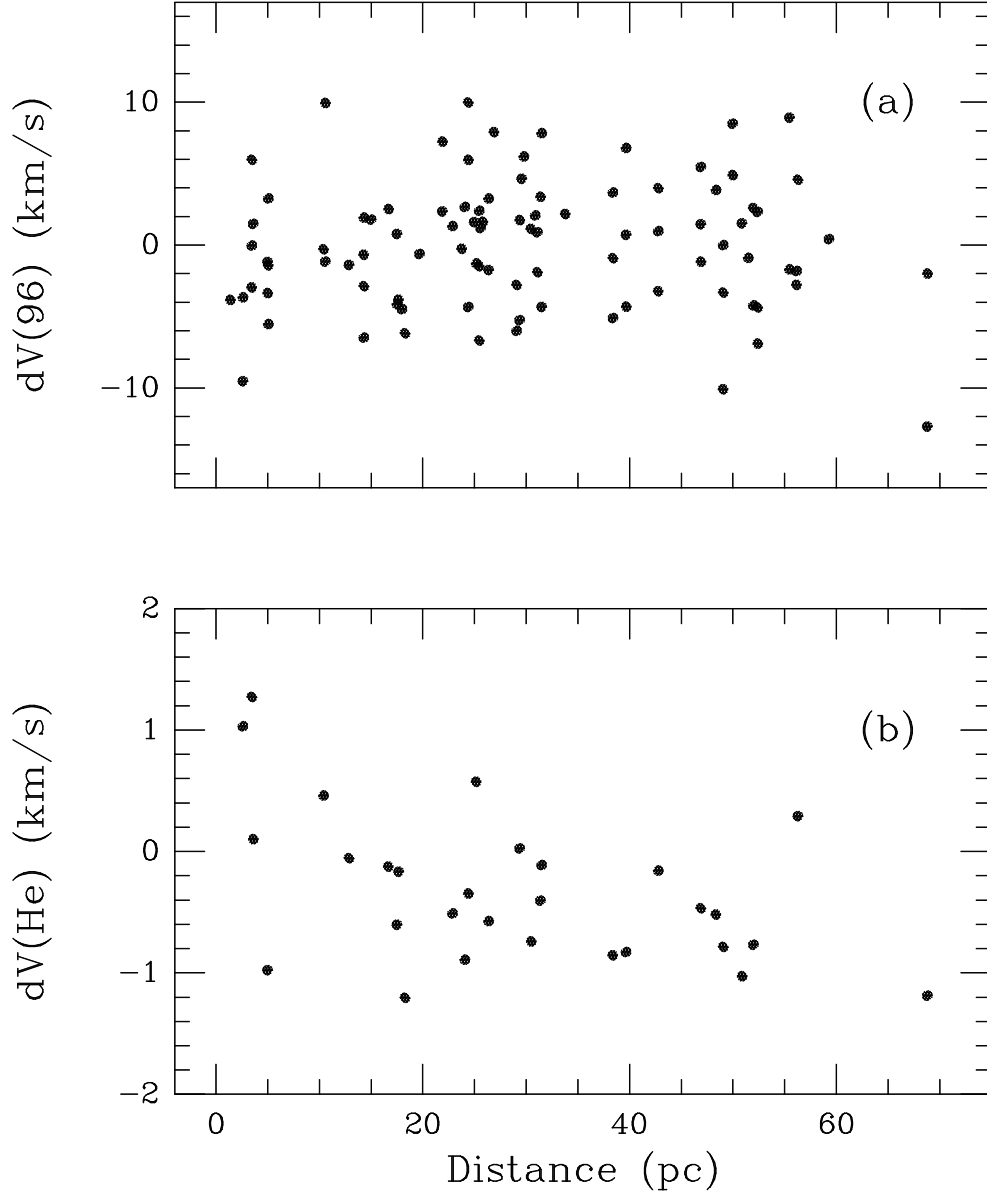


Fig. 1.— (a) Dispersion ( $dV_i(96)$ ) of component velocities in the rest frame of the CLIC as defined by  $\vec{V}_{\text{flow}}(96)$  (see Table 1). (b) Plot of  $dV_i(\text{He})$  versus star distance, for components within  $1.5 \text{ km s}^{-1}$  of  $\vec{V}_{\text{flow}}(\text{He})$  (i.e.  $|dV_i(\text{He})| < 1.5 \text{ km s}^{-1}$ ).

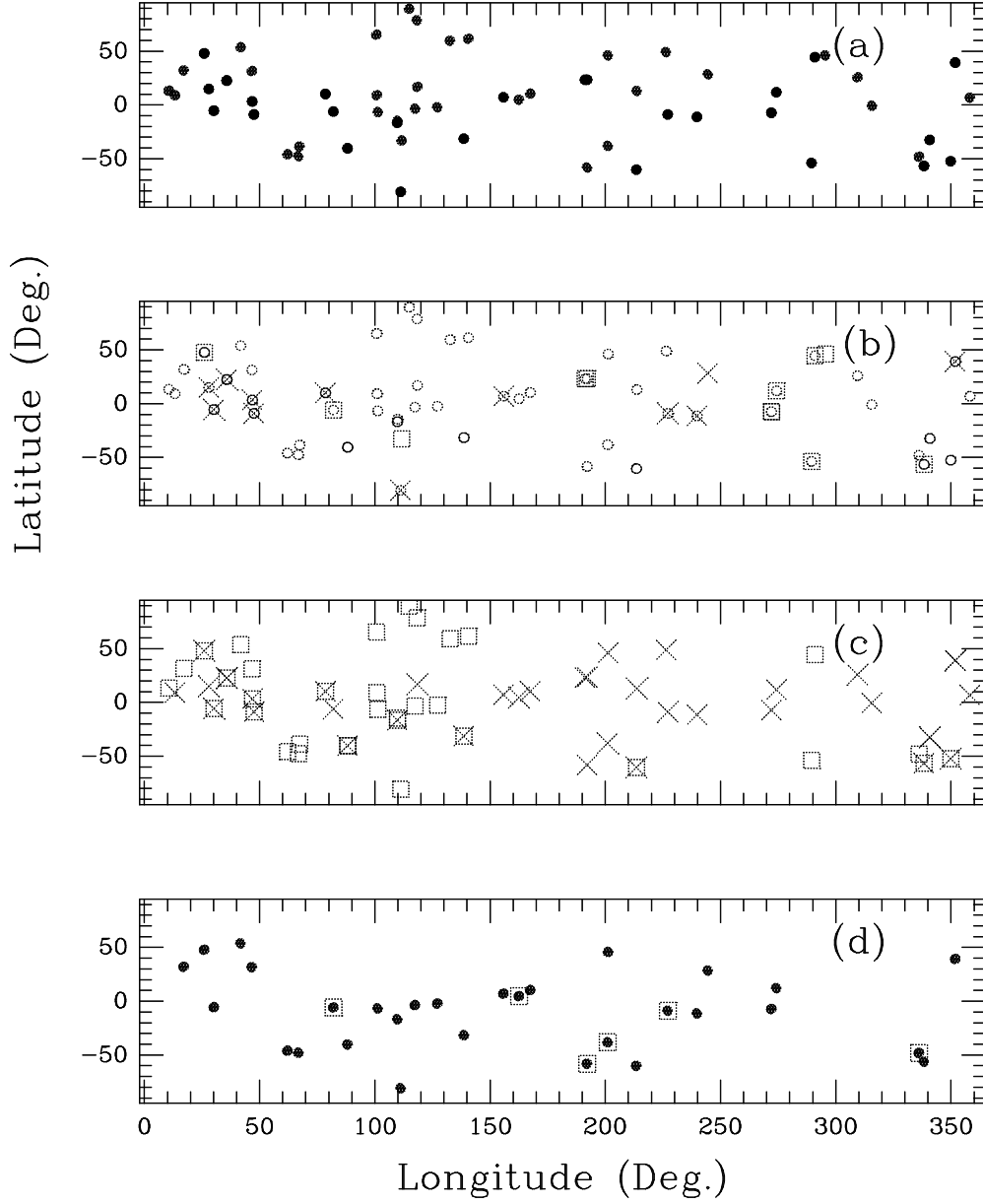


Fig. 2.— (a) The galactic coordinates of the background stars used to derive  $\vec{V}_{\text{flow}}(96)$  (Table 1)1 (b) Same stars as in (a), but coded for  $dV_i(96)$ : circle –  $|dV_i(96)| < 5 \text{ km s}^{-1}$ ; box –  $dV_i(96) > 5 \text{ km s}^{-1}$ ; cross –  $dV_i(96) < -5 \text{ km s}^{-1}$ . Stars with multiple components show more than one symbol. (c) The stars for which  $|dV_i(96)| < 5 \text{ km s}^{-1}$  are coded for the sign of  $dV_i(96)$ : box –  $dV_i(96) > 0 \text{ km s}^{-1}$ ; cross –  $dV_i(96) < 0 \text{ km s}^{-1}$ . Stars with components in each range show both symbols. (d) The galactic coordinates of the 30 stars with components showing  $|dV_i(\text{He})| < 1.5 \text{ km s}^{-1}$ . Boxes surround the positions of stars within 15 pc.

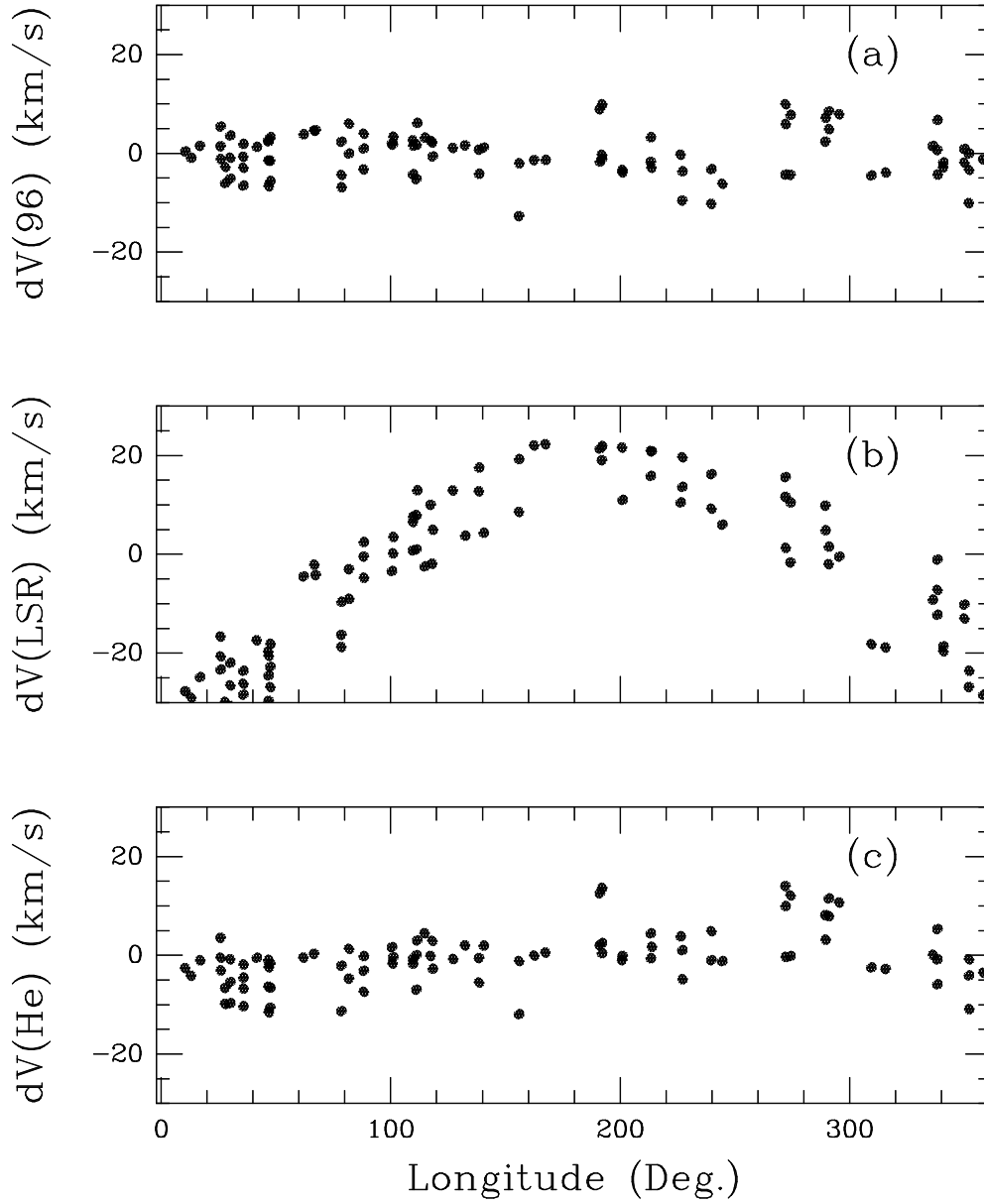


Fig. 3.— (a)  $dV_i(96)$  plotted against galactic longitude for the restricted sample of stars. (b)  $dV_i(\text{LSR})$  plotted against galactic longitude for same stars. The sinusoidal appearance shows that the ISM within 30 pc of the Sun is not near the rest velocity of the LSR (e.g. also see Frisch (1995)). (c)  $dV_i(\text{He})$  plotted against galactic longitude for same stars.

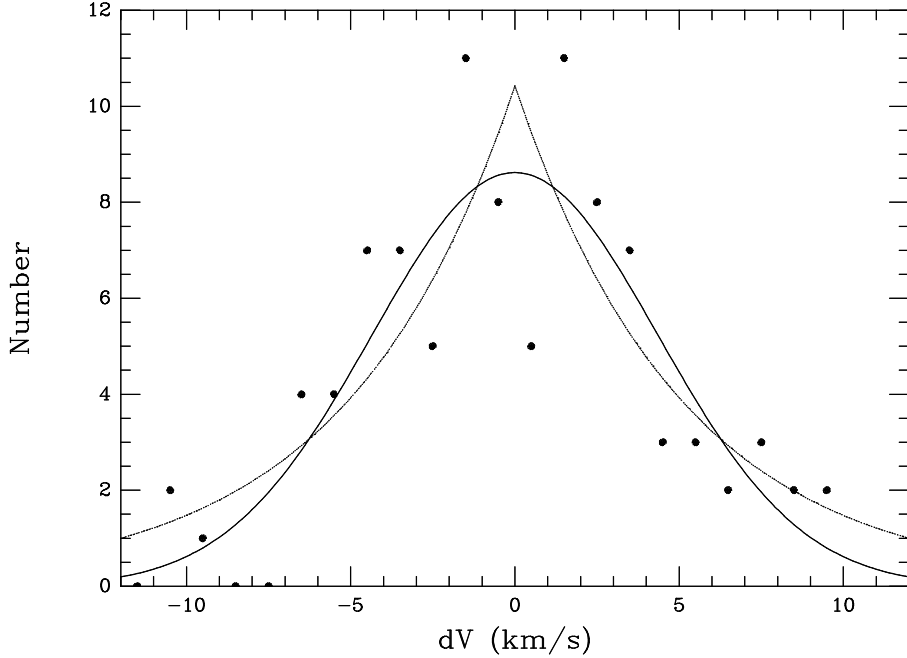


Fig. 4.— Histogram of  $dV$  values, calculated used  $\vec{V}_{\text{flow}}(96)$ . A best-fit exponential component distribution (dotted line) is overplotted for  $\eta=5.1$  (Equation 5). The best-fit Gaussian distribution (solid line) for these same components, with  $b=6.2 \text{ km s}^{-1}$ , is also shown (Equation 4).

Fig. 5.— The  $\vec{V}_{\text{flow}}(96)$  upstream direction in the LSR ( $l^{\text{II}}=1.8^\circ$ ,  $b^{\text{II}}=-3.2^\circ$ ) is shown plotted on a map of 21 cm emission integrated over the velocity range  $-450$  to  $400 \text{ km s}^{-1}$ , with the  $\text{H}^\circ$  Loop I faintly visible (Hartmann & Burton 1997). The Loop I position in 408 MHz radio continuum emission is overplotted as two lines (from Berkhuijsen 1971; Haslam et al. 1982). The LSR upstream direction of  $\vec{V}_{\text{flow}}(96)$  (dot) is  $\sim 20^\circ$  from the tangential direction of Loop I, consistent with a CLIC origin associated with either an expanding Loop I superbubble, or an outflow from the Sco-Cen Association (e.g. Frisch 1995).

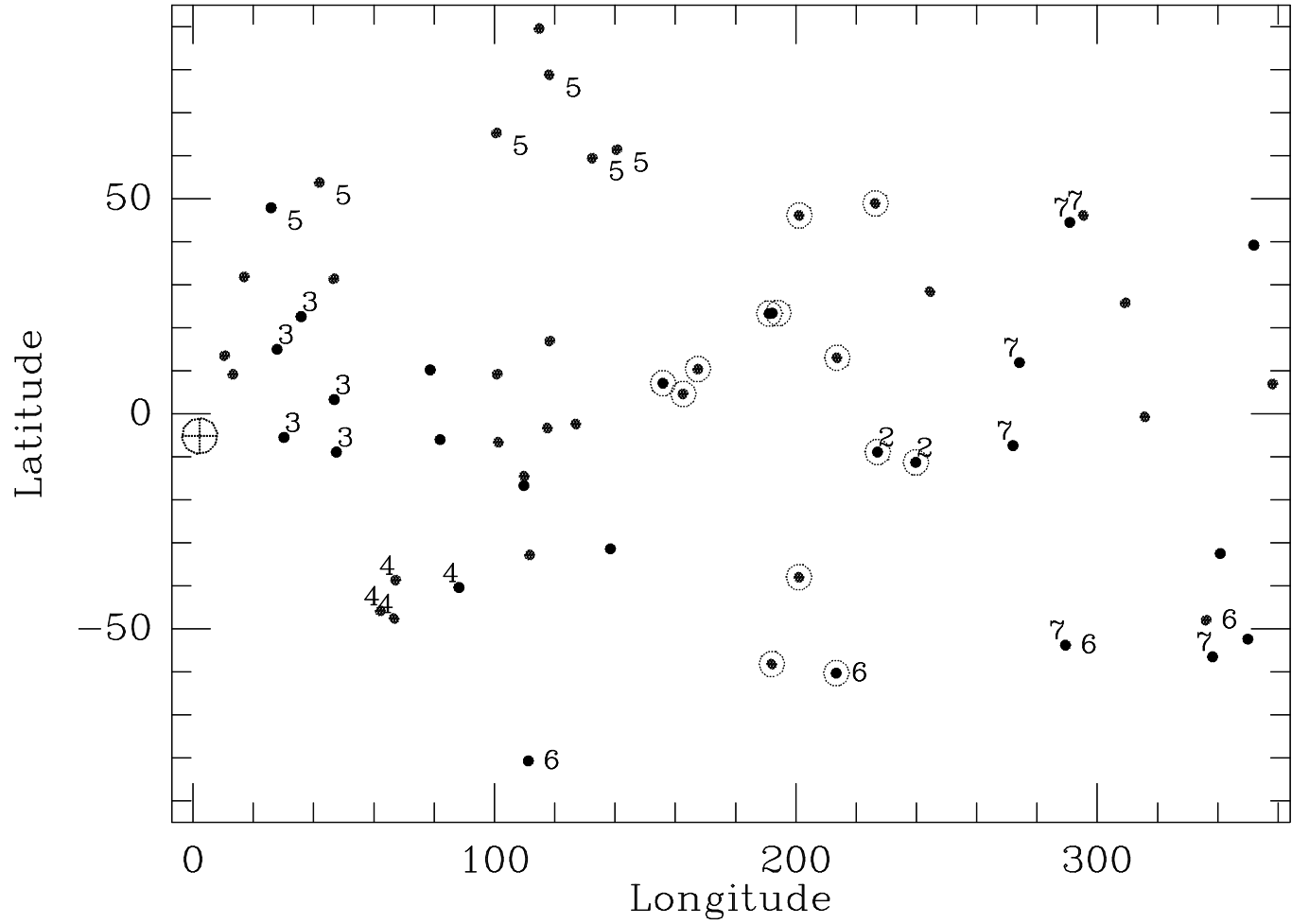


Fig. 6.— The Clouds listed in Table 4 are shown plotted against positions of stars in the restricted sample. Positions of stars showing Cloud 1 components are circled, and other clouds are identified by cloud number. The LSR upstream direction of  $\vec{V}_{\text{flow}}(96)$  is identified by the circled cross.

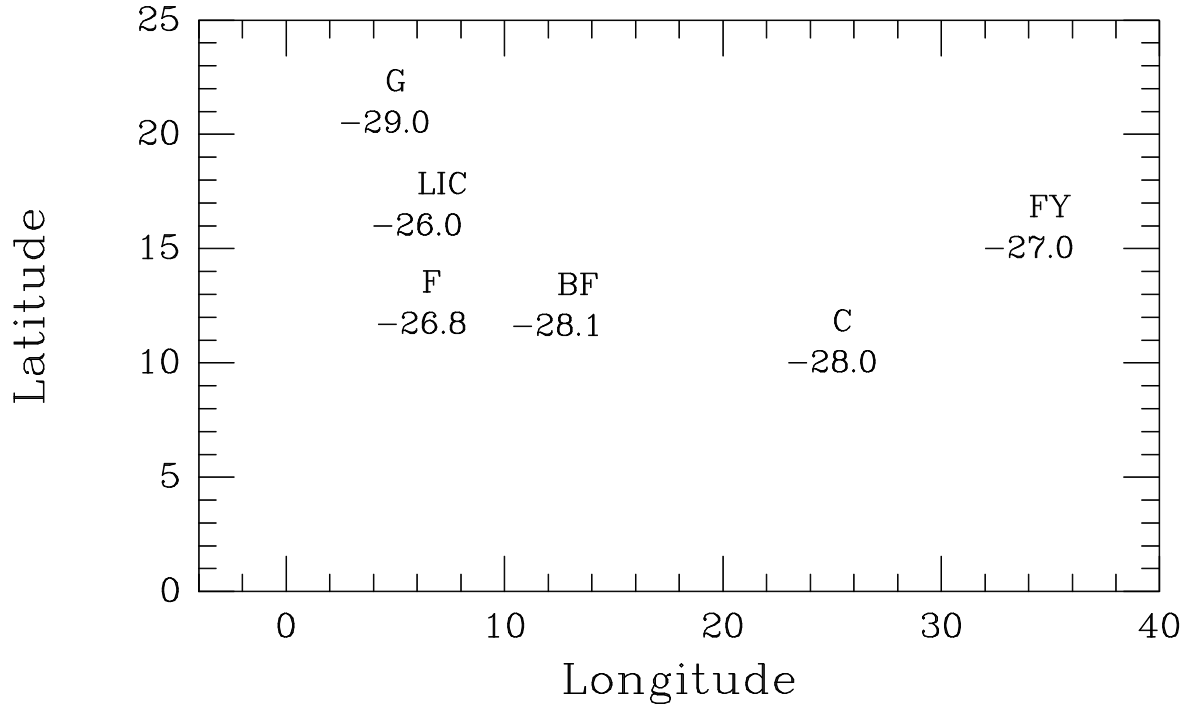


Fig. 7.— Heliocentric upstream directions for various bulk velocity vectors found for nearby ISM are plotted. Labels and data for individual vectors are presented in Table 5.

This figure "fig5.gif" is available in "gif" format from:

<http://arxiv.org/ps/astro-ph/0203093v1>